Journal of Anatomy

J. Anat. (2013) **223**, pp603–609 doi: 10.1111/joa.12113

The dermal arteries of the human thumb pad

S. H. Geyer, M. M. Nöhammer, I. E. Tinhofer and W. J. Weninger

Medical University of Vienna, Centre for Anatomy and Cell Biology, Vienna, Austria

Abstract

The arteries of the skin have been postulated to form a profound plexus at the dermal/hypodermal junction and a superficial plexus in the papillary dermis. Our article aims to rebut this concept and to provide an alternative description of the arrangement of the dermal arteries. Employing a novel technique, we produced digital volume data (volume size: 2739 × 2054 × 3000 μm^3; voxel size: 1.07 × 1.07 × 2 μm^3) from biopsies of the skin of the thumb pads of 15 body donors. Utilizing these data, we analysed the arrangement of the dermal arteries with the aid of virtual re-sectioning tools, and, in three specimens, with high-quality three-dimensional (3D) surface models. In all specimens we observed a tree-like ramification of discrete dermal arteries. The terminal branches of the arterial trees gave rise to the ascending segments of the capillary loops of the dermal papillae. None of the specimens showed a superficial arterial plexus. This suggests that the skin of the human thumb pad can be split in discrete 'arterial units'. Each unit represents the zone of the papillary dermis and epidermal/dermal junction, to which blood is supplied exclusively by the branches of a single dermal artery. The concept of dermal arterial units is in contrast to all existing descriptions of the architecture of the dermal arteries. However, whether it can be transferred to the skin of other body parts, remains to be tested. Likewise, the consequences of arterial units for understanding the mechanisms of wound healing and the appearance and genesis of skin diseases remain to be examined.

Key words: blood supply; high resolution episcopic microscopy; skin; superficial arterial plexus; three-dimensional reconstruction.

Introduction

The skin has three layers: the epidermis; the dermis, which is composed of a narrow superficial papillary and a thicker and more profound reticular layer, and the hypodermis. Whereas the epidermis does not contain blood vessels, the dermis and hypodermis are extensively vascularized. The arrangement of the blood vessels, especially of the arteries, is essential for the physiological function of the entire skin.

Many diseases affect the topology of dermal blood vessels, e.g. Raynaud's disease, erythromelalgia, cutis marmorata, nevus flammeus and diabetes mellitus (Requena & Sangueza, 1997; Mork et al. 2002; Raffetto, 2009). To research the genesis and the functional consequences of cutaneous pathologies it is essential to define the topological aberrations dermal blood vessels show in diseased skin areas. The basis for such an analysis is a detailed description of the arrangement of the dermal arteries in the unaltered skin.

Correspondence
Wolfgang J. Weninger, Centre for Anatomy and Cell Biology, Medical University of Vienna, Waehringerstr. 13, A-1090 Vienna, Austria.
E: Wolfgang.Weninger@meduniwien.ac.at

Accepted for publication *28 August 2013*
Article published online *20 September 2013*

Anatomical and dermatological textbooks and scientific articles postulate the existence of two nearly horizontal arterial plexus in the human skin (Spalteholz, 1927; Williams et al. 1989; Braverman, 2000; Kanitakis, 2002; Fritsch, 2009): A profound arterial plexus (deep arterial plexus, subcutaneous arterial plexus) and a superficial (subpapillary) arterial plexus. The profound plexus is located at the dermal/hypodermal junction. It is fed by branches of the large subcutaneous arteries and gives rise to arteries that travel vertically through the reticular dermis to feed the superficial plexus. This plexus is located in the papillary dermis and gives rise to capillaries, which enter the dermal papillae.

Each dermal papilla receives a capillary (Horstmann, 1957; Ikeda et al. 1991; Sangiorgi et al. 2004). Once inside the papilla, the capillary ascends towards the tip of the papilla, turns, and descends to drain into a venous plexus, which is again formed in the papillary dermis (Spalteholz, 1927; Horstmann, 1957; Yen & Braverman, 1976; Inoue, 1978; Braverman, 2000; Kanitakis, 2002).

The concept of a superficial arterial plexus was developed on the basis of studies utilizing sophisticated imaging techniques. In particular the Spalteholz technique, the corrosion cast technique, and histological section-based 3D reconstruction techniques were employed (Spalteholz, 1927; Conrad, 1968; Inoue, 1978; Braverman et al. 1990). However, these

techniques have serious limitations, which may hinder the correct identification of connections of small blood vessels.

The Spalteholz and corrosion cast techniques require the perfusion of blood vessels. But selective perfusion of arteries down to the small branches is challenging and works best with fresh material, the access to which is limited. Furthermore, neither technique produces digital data volumes. Therefore separate visualization and analysis of arteries and veins as well as the creation of virtual re-sections cutting in various directions through the 3D models is impossible. As a consequence these techniques provide excellent 3D representations of blood vessel networks but have problems in permitting distinctions and topological analysis of arteries and veins in the context of complex three-dimensional (3D) vascular networks (Weninger & Geyer, 2009).

Histological section-based 3D reconstruction techniques provide digital volume data. But these data are derived from physical histological sections with a typical thickness of 5–10 μm. Thus the resolution of the data volumes is limited to 5–10 μm in a direction normal to the section plane. In addition, physical sections suffer from non-affine distortions introduced by the sectioning process. These distortions effectively hinder correct tracing of smaller sized arteries (Weninger & Geyer, 2009).

Having these technical limitations in mind, we decided to re-examine the arrangement of the dermal arteries of the thumb pad by using digital volume data produced with a novel high-resolution digital 3D imaging technique.

Material and methods

The skin of the thumb pads of 15 body donors (10 females, five males) was examined. The age at time of death was between 60 and 93 years (mean 77.5 years).

The corpses of the body donors were fixed following a protocol we routinely use to prepare corpses for dissecting classes. The bodies were perfused for a total of 5 days with a solution consisting of 4% carbolic acid and 0.5% formaldehyde. After perfusion, they were immersed in a solution consisting of 4.5% carbolic acid and 0.9% paraformaldehyde for 6–12 months.

Using 4-mm biopsy punches (Biopsy Punch, Stiefel®), biopsies were taken from the centre of the distal half of the thumb pads of the fixed corpses. The height of the biopsy cylinder was approximately 3 mm. A biopsy from the right thumb pad of eight body donors and from the left thumb pad of seven body donors was taken. Biopsy material was stored in 4% neutral buffered formaldehyde until it was processed for volume data generation.

Digital volume data were generated with the high resolution episcopic microscopy (HREM) technique (Weninger et al. 2006; Mohun & Weninger, 2010). The specimens were rinsed in running tap water for 1–3 days. Then they were dehydrated in a series of ethanols of increasing concentrations. Each specimen stayed 48 h in 50%, 48 h in 70%, 20 h in 80%, 20 h in 90%, and 20 h in 96% ethanol. The ethanols contained 0.4 g eosin (Eosin spritlöslich, Waldeck) per 100 mL.

After dehydration, the specimens were infiltrated by putting them into solution A of the JB-4 Plus® embedding kit, which contained 1.25 g catalyst (benzoyl peroxide, plasticized) and 0.4 g eosin 100 mL^{-1}. They were left in this solution for 1–2 days. The solution was changed twice. After infiltration, the specimens were transferred into embedding moulds and embedded in eosin-dyed resin following a standardized embedding protocol (Mohun & Weninger, 2012a). After putting block holder on top of the moulds, they were sealed airproof for at least 2–3 days. After this the blocks were stored under room conditions until they were processed further.

Digital data generation again followed a standard protocol (Weninger et al. 2006; Mohun & Weninger, 2012b). With the aid of our HREM apparatus, a series of about 1200–2500 inherently aligned digital images was created. The images showed the subsequently exposed block surfaces during the sectioning of the block. Pixel size of the images was 1.07×1.07 μm^2. The field of view was 2739×2054 μm^2. Section thickness was 2 μm.

Image series were transferred to a PC workstation (two processors 2.67 GHz, 72 GB RAM, Nvidia GeForce GTX 580 graphic card). The PC operated Windows7 and the software package AMIRA® (Visualization Sciences Group). After loading an image series into AMIRA, the images were virtually stacked and converted to volume data with a voxel size of $1.07 \times 1.07 \times 2$ μm^3.

The large arteries of the hypodermis were identified in all specimens. Their branches and sub-branches were followed by scrolling forwards and backwards through the images composing the data volume. If required, virtual re-sections were defined, which cut through the data volume approximately perpendicular to the longitudinal axis of the artery that was followed. The course of the artery was then traced by scrolling through subsequent re-sections.

For better visualization, low-quality 3D surface models were created. The branching points of the dermal arteries were labelled with small circles. The distances between labelled branching points were then connected using the automated interpolation tool of the AMIRA® software (Fig. 1).

The dermal arteries of three specimens were analysed more carefully. Proper high-quality 3D surface models were created by tracing the outlines of the arteries in every single section of the data volume. The models were then analysed by employing the surface model visualization tools of AMIRA®.

The high-quality 3D models were also used for measuring the diameters of the arteries. For this a protocol was used that was originally developed for measuring the diameter of embryonic arteries (Weninger et al. 2009; Geyer et al. 2012). In short, virtual re-slices were defined, which cut perpendicularly to the longitudinal axis through the artery segment we intended to measure. In the resection image the perimeter of the lumen of the artery was measured. Then the diameter was calculated from the perimeter. The study was conducted with approval of the local ethics commission.

Results

In a first step, we created high-resolution digital volume data and 3D surface-rendered models of the arteries occupying a $2739 \times 2054 \times 3000$ μm^3 section of three human thumb pads. The 3D models showed similar patterns, as follows.

Relatively large arteries with diameters between 150 and 242 μm were located at the hypodermal/dermal junction. They were at the very 'bottom' and partly outside of the

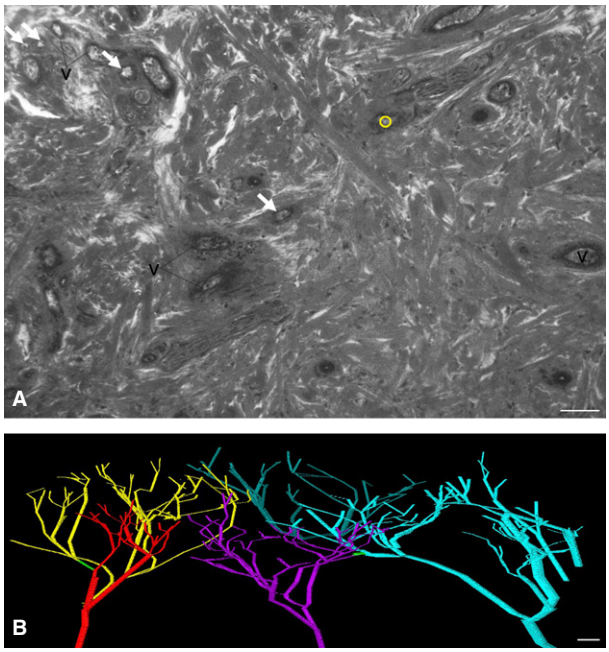

Fig. 1 Analysing dermal arteries by labelling branching points and interpolating the distances in between. (A) Central section of a HREM image through the dermis. One branching point of arteries is visible and labelled with a small yellow circle. Arteries, which are visible but do not ramify in this image, are indicated with arrows. v, veins. (B) Low-quality 3D models created by interpolating the distances between labelled branching points. Five different arterial trees are displayed. A single anastomosis (green) connects branches of two neighbouring trees. The models do not provide information about the dimensions of the blood vessels. Scale bars: 100 μm.

digital data volumes. In one specimen one of these arteries entered the reticular dermis, formed an arch and ran back to the hypodermal/dermal junction (Fig. 2A).

Within a data volume, two to three arteries with lumen diameters between 100 and 120 μm arose from respectively the large hypodermal arteries and the large hypodermal artery that arched into the dermis. These arteries ascended towards the dermal/epidermal junction and started ramifying in a tree-like manner at approximately halfway on their way through the reticular dermis. These arteries had 5–11 generations of branches (Fig. 2).

The final generation of branches had a lumen diameter of 8–15 μm and gave rise to three to seven blood vessels that ascended towards the lower tips of the papillae. Some of these vessels directly entered a papilla and formed the ascending segment of its capillary loop. Some vessels split in two or three at the level of the lower tip of neighbouring papillae and thus formed the ascending segments of neighbouring capillary loops.

The branches of the arterial trees, which were located within the reticular dermis, gave rise to capillary-sized blood vessels. Occasionally these vessels started to form highly complex networks in the epineurium of larger nerve stems, or joined the ducts of sweat glands on their way to the hypodermis (Figs 2 and 3A).

The terminal capillary loops stemming from a single arterial tree entered the dermal papillae of an irregularly-, but roughly oval-shaped area. The major diameter of the oval measured between 1300 and 2000 μm. The minor diameter measured between 750 and 1200 μm. The marginal terminal branches and capillary loops of neighbouring arterial trees interdigitated. The width of the zone of interdigitation was between 100 and 250 μm (Fig. 3).

In two of the three specimens we identified arterio-arterial anastomoses. In one specimen, we identified three anastomoses, two were between neighbouring arterial trees. They connected branches of the 4th to 5th generation and were located approximately 520 and 380 μm below the lower tips of the epidermal papillae, respectively. The diameter of their lumina measured 12 μm and 14 μm, respectively. One was between two branches of an arterial tree, from which only a few branches were located inside the data volume (Fig. 4).

In a second specimen we also identified three anastomoses. One anastomosis connected branches of the 2nd and 3rd generation of two nneighbouring arterial trees. It was short, had a diameter of 33 μm and was located approximately 1 mm below the lower tip of the epidermal papillae. The other two anastomoses connected arteries of the second last generation. They had a lumen diameter of 8–10 μm. One connected arteries of neighbouring arterial trees. The other connected two branches stemming from the same arterial tree (Fig. 4). The third specimen did not show any anastomosis.

The information we gained from the analysis of the 3D models enabled us in a second step to analyse the topology of the dermal arteries of an additional 12 specimens in a much quicker way. While scrolling through the HREM data in various re-slice planes, we only labelled the branching points of the arteries and used software tools to connect them automatically. This dramatically reduced the time needed to analyse a single specimen, enabling higher numbers of biopsies to be analysed. The results of these analyses confirmed the small number of anastomoses per specimen (no anastomoses in three specimens, 1–4 anastomoses in eight, and 8 anastomoses in one) and the tree-like arrangement of the dermal arteries.

Discussion

We provide a detailed description of the architecture of the arteries of the dermis of the human thumb pad. Our results are based on the analysis of high-resolution digital volume data of 15 specimens. From three specimens we created and analysed high-quality virtual 3D models. Twelve specimens were analysed by scrolling through the digital data volumes in various virtual re-section planes and by creating 'low-quality' 3D surface models. This proved to be sufficient

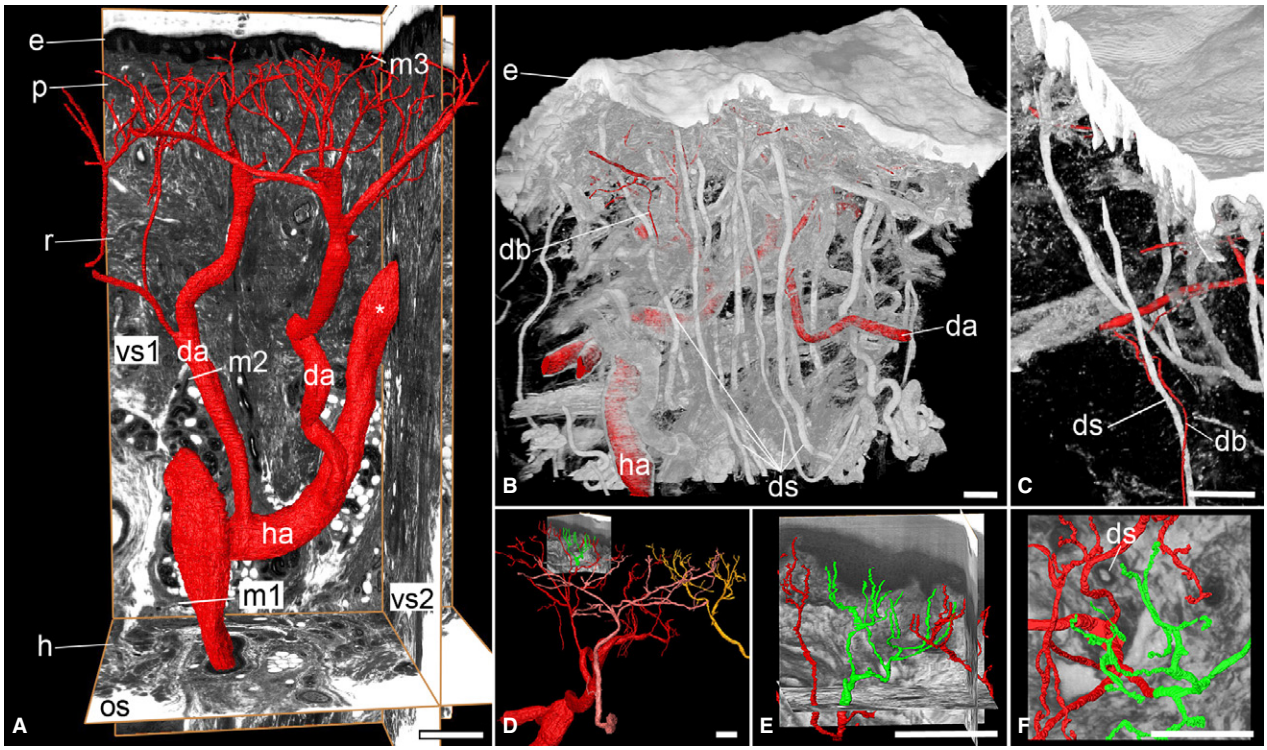

Fig. 2 Topology and branching of dermal arteries (da). High-quality 3D models. (A) Tree-like ramification. Surface 3D models of the lumina of the arteries in red. The ascending segments of the capillary loops are not visualized. Models are in front of an original HREM section (os) and two virtual re-sections (vs1, vs2) cutting through the HREM data. Note the positions (m1, m2, m3), at which diameters were measured. Note also the hypodermal artery (ha) that arches into the dermis (asterisk). e, epidermis; p, papillary layer of dermis; r, reticular layer of dermis; h, hypodermis. (B,C) Branches of dermal arteries (db) accompanying ducts of sweat glands (ds). Volume-rendered 3D model, combined with surface-rendered 3D models of arterial lumina. The stratum lucidum and stratum corneum of the epidermis are not visualised. (D-F) Terminal branches. Only the ascending segments of the capillary loops around the greenish highlighted segment of the red arterial tree are displayed. Different trees of dermal arteries are featured in (D) in red, pink, and yellow. (E,F) Terminal branches of the dermal arteries, (F) from a top view. The branches appear as if possibly forming a plexus. Scale bars: 100 μm.

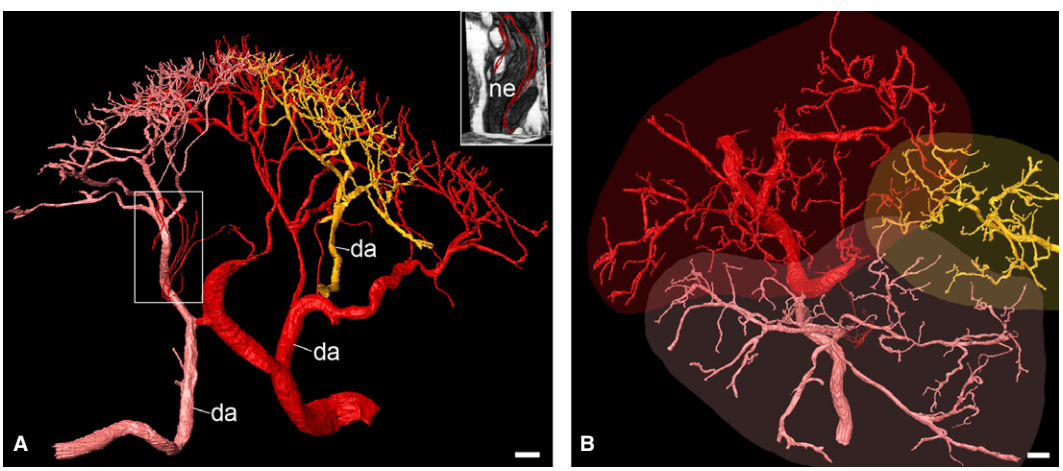

Fig. 3 Arterial units of the dermal/epidermal junction. Surface-rendered high-quality 3D models of three neighbouring arterial trees (red, pink, yellow). Larger parts of the yellow artery tree (da) are outside the data volume. (A) View from lateral. The boxed area is displayed in the insert in combination with two virtual resection planes. Note the capillaries, which supply a large nerve (ne) of the reticular dermis. (B) View from top. Note the schematically plotted extension of the arterial units. The capillaries supplying the nerve are outside the direct projection of the borders of the corresponding arterial unit. Scale bars: 100 μm.

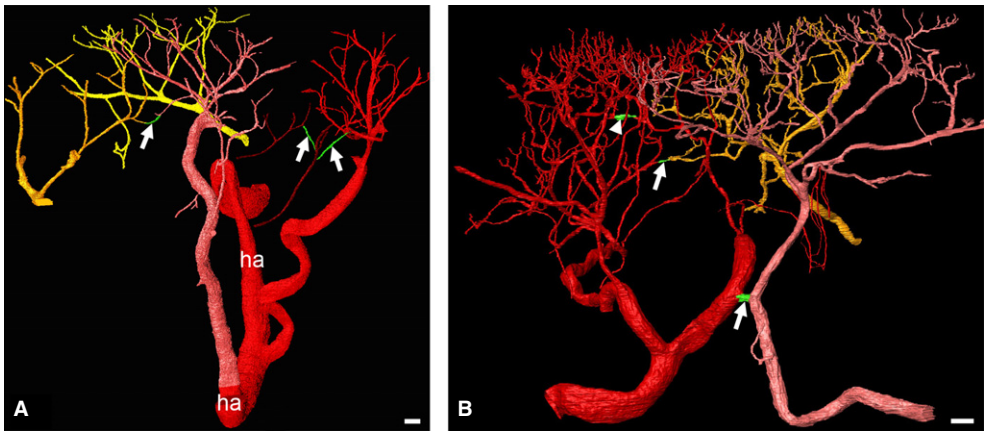

Fig. 4 Arterio-arterial anastomoses (green). Surface-rendered high-quality 3D models of neighbouring arterial trees. The projection view of the 3D models suggests multiple, plexus-like connections between the branches of the last generations. (A) Specimen with three anastomoses. The ascending segments of the capillary loops are not displayed. Only a few branches of the purple arterial tree are inside the data volume. Neighbouring arterial trees are displayed in red, pink, purple, dark yellow and bright yellow. ha, hypodermal artery. (B) Different specimen, also with three anastomoses. Two anastomoses connect branches of different arterial trees (arrows). One anastomosis is formed between branches of the red artery tree (arrowhead). Scale bars: 100 μm.

for counting the number of arterio-arterial anastomoses and for analysing the ramification patterns of the dermal arteries.

The most striking result is that none of our specimens had a superficial (subpapillary) arterial plexus. In all specimens, relatively thick dermal arteries arise from the profound (subcutaneous) arterial plexus and ramify in a tree-like manner until they form the ascending segment of the capillary loops of the papillae. This is in strong contradiction to all existing descriptions (Inoue, 1978; Ikeda et al. 1991; Braverman, 1997, 2000).

Our findings suggest that the papillary dermis and epidermis of the thumb pad can be split in 'arterial units'. To each unit, oxygen and nutrients are chiefly supplied by one of the arteries, which arise from the profound arterial plexus. The size of one unit is approximately 0.77–1.88 mm^2. Neighbouring units overlap.

We observed only a few anastomoses between the branches of the single dermal arteries and between branches of the arteries of neighbouring arterial units. Most of these anastomoses were small. We therefore assume that they do not permit the exchange of significant amounts of blood. Consequently, our results not only indicate that there is no superficial arterial plexus in a morphological sense, but also that there is no superficial arterial plexus in a functional sense.

Technical constraints prevented us from performing a comprehensive analysis of the profound arterial plexus. We were only able to create digital data volumes of 2739 × 2054 × 3000 μm^3. This data size allows the visualization of the epidermis, dermis, hypodermal/dermal junction, and the most superficial parts of the hypodermis of a skin area of approximately 2.7 × 2 mm^2. Therefore it does not permit the visualization of a wide-meshed arterial plexus in the hypodermis. Hence, we can only speculate that the relatively large arteries we observed are part of such a plexus.

In this study we focused on tracing and analysing large and small arteries. Except for the capillary loops of the papillae, we did not conduct a systematic analysis of the capillaries beause tracing capillaries in HREM data is extremely time-consuming. However, we noticed the formation of complex capillary networks in the epineurium of larger dermal nerve bundles. We therefore briefly report that such formations do exist, but do not provide a more detailed analysis of the architecture and distribution of these networks.

We only analysed thumb pads of people older than 59 years. This is important because the arrangement of the arteries differs between various skin regions and younger people might show differences in the architecture of the dermis and its arteries (Spalteholz, 1927; Inoue, 1978; Ikeda et al. 1991). Thus, the information we provide in this article, as well as the concept of dermal arterial units, is only proved for the skin of the thumb pad of seniors. Whether other skin regions or the thumb pads of children show a similar arrangement remains to be researched in follow-up studies.

Detailed information about the architecture of the dermal arteries in the healthy skin is essential for interpreting the patterns of the arteries forming in healing wounds and skin grafts. Therefore, to the extent that all normal skin vascularization should follow the thumb pattern, research in neovascularization of skin flaps or skin replacement materials may profit from our data. As examples of clinical and physiological implications, it would be tempting to speculate upon the relationship between the appearance of rashes and the existence of arterial units, or on their role in skin temperature regulation. Regulation of skin temperature involves modulation of blood flow. But modifying

blood flow to a larger area of the skin by contraction or dilation of the dermal arteries would involve synchronous activity of every single dermal unit of the respective area. As this is unlikely, the temperature of the body might be regulated at the level of the central arteries of angiosomes.

However, we would like to emphasize that these ideas are only speculative. Exploring the definitive physiological and clinical consequences of our findings was not the aim of this anatomical study, and must be done in careful follow-up studies.

The reason why our results contradict existing concepts of a superficial arterial plexus might be partly a technical one. Existing studies visualized the dermal arteries with the Spalteholz technique (Spalteholz, 1911), the corrosion cast technique (with and without scanning electron microscopy) (Conrad, 1968; Inoue, 1978; Ikeda et al. 1991; Hasegawa et al. 2001), optical coherence microscopy (OCT; Zhang et al. 2011; Dalimier & Salomon, 2012), histological section-based 3D reconstruction techniques, and traditional histological section techniques (Braverman et al. 1990). But visualizing the extensively branching small arteries of the superficial dermis, which are surrounded by a venous plexus that is filled by the descending segments of the arterial loops of the papillae, is extremely challenging. Although all the above techniques are highly sophisticated, none it optimal for this task.

We employed a novel episcopic 3D imaging technique called high-resolution episcopic microscopy (HREM; Weninger et al. 2006). HREM creates digital volume data with a voxel size of 1.07 $\times$ 1.07 $\times$ 2 μm. The data are basically virtual stacks of series of inherently aligned digital images of almost histological quality. The combination of high data quality, inherent alignment of the digital images, relatively high spatial resolution, and a field of view of 2739–2054 μm^2, permitted the identification and the precise 3D tracing of blood vessels throughout a sufficiently large segment of the entire dermis. This is at least true for blood vessels down to the size of the terminal branches of the arterial trees, including the ascending segments of the capillary loops. However, small capillaries could not be traced with certainty.

High resolution episcopic microscopy data generation is quick and simple. In contrast, HREM data analysis is slow and requires expert knowledge. Especially the creation of surface-rendered 3D models is exorbitantly expensive in terms of time. For this reason, we only created 3D models of the arteries of three specimens and did not outline the ascending segments of the capillary loops in all specimens.

In 12 specimens we did not create high-quality 3D models but instead explored the arrangement of the dermal arteries by scrolling through the HREM volume data in different virtual re-section planes and producing low-quality surface models. Such analyses, although still time-consuming, are much quicker. They also revealed a tree-like ramification of the dermal arteries and only a small number of arterio-arterial anastomoses. Thus we feel confident in challenging the existence of a superficial arterial plexus in the dermis in – at least – the thumb-pad of adult humans.

References

Braverman IM (1997) The cutaneous microcirculation: ultrastructure and microanatomical organization. *Microcirculation* **4**, 329–340.

Braverman IM (2000) The cutaneous microcirculation. *J Investig Dermatol Symp Proc* **5**, 3–9.

Braverman IM, Keh A, Goldminz D (1990) Correlation of laser Doppler wave patterns with underlying microvascular anatomy. *J Invest Dermatol* **95**, 283–286.

Conrad MC (1968) Abnormalities of the digital vasculature as related to ulceration and gangrene. *Circulation* **38**, 568–581.

Dalimier E, Salomon D (2012) Full-field optical coherence tomography: a new technology for 3D high-resolution skin imaging. *Dermatology* **224**, 84–92.

Fritsch P (2009) (ed.) Aufbau und Funktionen der Haut. In: *Dermatologie und Venerologie für das Studium*. Heidelberg: Springer Medizin Verlag.

Geyer SH, Maurer B, Potz L, et al. (2012) High-resolution episcopic microscopy data-based measurements of the arteries of mouse embryos: evaluation of significance and reproducibility under routine conditions. *Cells Tissues Organs* **195**, 524–534.

Hasegawa K, Pereira BP, Pho RW (2001) The microvasculature of the nail bed, nail matrix, and nail fold of a normal human fingertip. *J Hand Surg Am* **26**, 283–290.

Horstmann E (1957) Blutgefäße der Haut. In: *Handbuch der Mikroskopischen Anatomie des Menschen* (ed. Möllendorff Wv), pp. 198–207. Berlin: Springer.

Ikeda A, Umeda N, Tsuda K, et al. (1991) Scanning electron microscopy of the capillary loops in the dermal papillae of the hand in primates, including man. *J Electron Microsc Tech* **19**, 419–428.

Inoue H (1978) Three-dimensional observations of microvasculature of human finger skin. *Hand* **10**, 144–149.

Kanitakis J (2002) Anatomy, histology and immunohistochemistry of normal human skin. *Eur J Dermatol*, **12**, 390–399; quiz 400–1.

Mohun T, Weninger WJ (2010) Episcopic Three-Dimensional Imaging of Embryos. In: *Imaging in Developmental Biology: A Laboratory Manual*. (eds Sharpe J, Wong R), pp. 765–776. New York: Cold Spring Harbor Laboratory.

Mohun TJ, Weninger WJ (2012a) Embedding embryos for high-resolution episcopic microscopy (HREM). *Cold Spring Harb Protoc* **2012**, 678–680.

Mohun TJ, Weninger WJ (2012b) Generation of volume data by episcopic three-dimensional imaging of embryos. *Cold Spring Harb Protoc* **2012**, 681–682.

Mork C, Kvernebo K, Asker CL, et al. (2002) Reduced skin capillary density during attacks of erythromelalgia implies arteriovenous shunting as pathogenetic mechanism. *J Invest Dermatol* **119**, 949–953.

Raffetto JD (2009) Dermal pathology, cellular biology, and inflammation in chronic venous disease. *Thromb Res* **123**(Suppl 4), S66–S71.

Requena L, Sangueza OP (1997) Cutaneous vascular anomalies. Part I. Hamartomas, malformations, and dilation of preexisting vessels. *J Am Acad Dermatol* **37**, 523–549.

Sangiorgi S, Manelli A, Congiu T, et al. (2004) Microvascularization of the human digit as studied by corrosion casting. *J Anat* **204**, 123–131.

Spalteholz W (1911) *Über das Durchsichtigmachen von Menschlichen und Tierischen Präparaten und Seine Theoretischen Bedingungen*. Leipzig: S. Hirzel Verlag .

Spalteholz W (1927) Blutgefäße der Haut. In: *Handbuch der Haut und Geschlechtskrankheiten* (ed. Jadassohn J), pp. 379–433. Berlin: Springer.

Weninger WJ, Geyer SH (2009) Three-dimensional (3D) visualisation of the cardiovascular system of mouse embryos and fetus. *Open Cardiovasc Imaging J* **1**, 1–12.

Weninger WJ, Geyer SH, Mohun TJ, et al. (2006) High-resolution episcopic microscopy: a rapid technique for high detailed 3D analysis of gene activity in the context of tissue architecture and morphology. *Anat Embryol* **211**, 213–221.

Weninger WJ, Maurer B, Zendron B, et al. (2009) Measurements of the diameters of the great arteries and semi-lunar valves of chick and mouse embryos. *J Microsc* **234**, 173–190.

Williams PL, Warwick R, Dyson M, et al. (1989) *Gray's Anatomy*. Edinburgh: Churchill Livingstone.

Yen A, Braverman IM (1976) Ultrastructure of the human dermal microcirculation: the horizontal plexus of the papillary dermis. *J Invest Dermatol* **66**, 131–142.

Zhang EZ, Povazay B, Laufer J, et al. (2011) Multimodal photoacoustic and optical coherence tomography scanner using an all optical detection scheme for 3D morphological skin imaging. *Biomed Opt Express* **2**, 2202–2215.